STRUCTURAL CONTROL AND HEALTH MONITORING
Struct. Control Health Monit. (2012)
Published online in Wiley Online Library (wileyonlinelibrary.com). DOI: 10.1002/stc.1483

Modelling and numerical simulations of vibrothermography for impact damage detection in composites structures

L. Pieczonka[1], F. Aymerich[2], G. Brozek[1], M. Szwedo[1], W. J. Staszewski[1,*,†] and T. Uhl[1]

[1]*Department of Robotics and Mechatronics, AGH University of Science and Technology, Al. Mickiewicza 30, 30-059 Krakow, Poland*
[2]*Department of Mechanical Engineering, University of Cagliari, 09123 Piazza d'Armi, Cagliari, Italy*

ABSTRACT

The paper investigates modelling aspects related to application of vibrothermography for detection of barely visible impact damage in composite structures. Low-velocity impact tests were performed to introduce multiple delaminations into carbon/epoxy composite plate. Damage severity was revealed using well-established non-destructive evaluation techniques. Vibrothermography was used subsequently to show good agreement with classical damage detection techniques. Following these experimental investigations, numerical simulations were performed to assess feasibility and sensitivity of vibrothermography for impact damage detection. Numerical results were validated using experimental data showing very good qualitative and encouraging quantitative agreement. The study demonstrates that virtual impact damage detection using vibrothermography can be performed as part of structural design to assess sensitivity of the method in real engineering applications. Copyright © 2012 John Wiley & Sons, Ltd.

Received 5 November 2011; Revised 11 January 2012; Accepted 14 January 2012

KEY WORDS: composite structures; vibrothermography; numerical modelling; finite element analysis (FEA); impact damage monitoring

1. INTRODUCTION

It is well-known that composite materials are susceptible to damage following an impact, which may occur during manufacture, service, or maintenance [1,2]. Impact damage may evolve into various forms before complete failure. Typical damage mechanisms include matrix ply cracking, fibre cracking, and delaminations between the plies. Barely visible impact damage (BVID) is of particular concern in aerospace industries. Reliable methods are needed to detect and monitor BVID evolution. A number of different methods have been developed for damage detection in composite structures for the past 40 years [1–3]. These include visual inspection, passive and active approaches based on ultrasonic signals, liquid penetrant testing, eddy current-based methods, radiographic methods, and thermographic methods. The success of these methods in industrial applications often depends on three major factors. First, interpretation of complex damage detection data should be eliminated. This is because maintenance procedures are often undertaken by modestly qualified technicians. Second, baseline measurements, i.e. data representing a 'no damage' condition, should be avoided. Damage detection based on baseline data needs excessive databases and often requires measurements that are not possible in practice. Third, logistics and practicality often require damage detection methods that do not need large transducer networks. Thermography [4] is one of the non-destructive techniques that meet these requirements. Of special interest among the thermographic approaches is—because of its efficiency—vibrothermography.

*Correspondence to: Staszewski Wieslaw, AGH University of Science and Technology, Department of Robotics and Mechatronics, Al. Mickiewicza 30, 30–059 Krakow, Poland.
†E-mail: w.j.staszewski@agh.edu.pl

The method monitors heat produced by damage under vibration and/or ultrasonic excitation. Vibrothermography has been gaining more attention in various damage detection investigations [5–9]. This is because of several factors that are necessary for reliable measurements, one of the most important of which is the availability of more efficient and affordable infrared cameras. The main issues of concern in industrial application of vibrothermography are still reproducibility and reliability of measurements [8]. Despite many research efforts, the mechanisms of vibration energy dissipation on damage are not yet fully understood but certainly depend on material and defect types [12,13]. Therefore, the exact amount of heat that is expected to dissipate on certain defects is not known *a priori*. Nevertheless, it is known that generated heat depends on frequency and position of excitation source [8,11].

The problem of virtual vibrothermographic testing is of great importance not only for better physical understanding but ultimately for improving practical aspects associated with the method. Virtual damage detection would allow a designer to estimate the capability of the method by assessing minimal defect size that could be detected. As a result more damage-tolerant design principle could be used and relevant maintenance schedules planned accordingly. Virtual damage detection would allow a maintenance engineer to customize damage detection setup and parameters before actual measurement field tests. The ultimate benefit would be associated with structural weight reduction and cost savings.

Virtual damage detection is inevitably related to physical modelling and numerical simulations. Previous work in this area include numerical studies on the efficiency of monoharmonic and chaotic ultrasonic excitations in generating heat around fatigue cracks [12–14], analysis of sources of energy dissipation (friction and plastic deformation) [13–16], analysis of crack detection in metallic components [11,17], and detection of fatigue damage in composite materials [18,19].

The main objective of this paper is to test the feasibility of performing virtual vibrothermographic test for impact damage detection in composites. In contrast to all previous studies, the current investigation presents a problem of numerical simulation of a real damage scenario in a carbon/epoxy prepreg plate.

The structure of the paper is as follows. Impact damage was introduced to a composite plate using a drop-weight impact test, as described in Section 2. The severity of damage was confirmed by classical non-destructive techniques, i.e. ultrasonic C-scan and penetrant-enhanced X-radiography (PEXR) as well as by vibrothermography as described in Section 3. Physical modelling and numerical simulations of low-velocity impact test are presented in Section 4. Physical modelling and numerical simulations of vibrothermographic test used for impact damage detection are reported in Section 5. Finally, the paper is concluded in Section 6. The study shows that virtual vibrothermographic test produces damage detection results that are in very good qualitative agreement with experimental results.

2. IMPACT DAMAGE IN COMPOSITES

2.1. Composite specimen

A rectangular composite plate with $[0_3/90_3]_s$ ply stacking sequence (Figure 1) had been used to demonstrate a case study. The dimensions of the plate were $120 \times 420 \times 2$ mm (Figure 2). The plate was cut from a laminate made up from Seal Texipreg® (Via Quasimodo, Legnano, Italy) HS160/Polymer Bound Acrylic Ester resin (REM) carbon/epoxy prepreg (61.5% fibre weight fraction) and cured in an

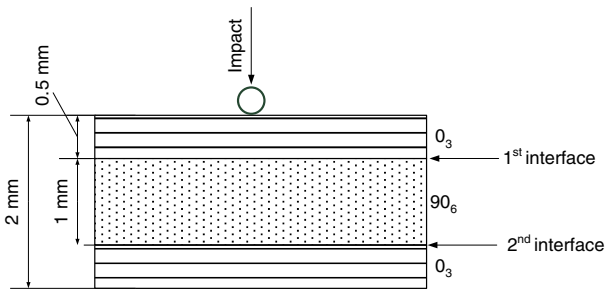

Figure 1. Details of the laminate structure and impact location.

DOI: 10.1002/stc

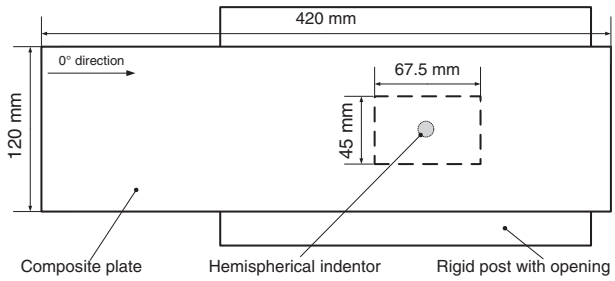

Figure 2. Impact test setup.

autoclave at a maximum temperature of 160 °C. The specimen was ultrasonically C-scanned prior to testing to assess the quality of the laminate and to exclude the presence of manufacturing defects.

2.2. Experimental impact tests

Damage was introduced in the composite plate using a drop-weight impact testing tower with a 2.3-kg impactor. The impactor was provided with a hemispherical indentor of 12.5 mm diameter and instrumented with a semiconductor strain–gauge bridge for dynamic load acquisition. A pneumatic catching mechanism was used to capture the impactor after the rebound so as to prevent multiple impacts on the plate. The velocity of the impactor immediately before and after the impact was obtained using an infrared sensor, whereas the contact force between impactor and specimen was measured using a semiconductor strain–gauge bridge bonded to the impactor rod. During testing, the composite specimen was simply supported on a steel plate with a rectangular opening 45×67.5 mm in size (Figure 2). The composite plate was subjected to two impacts at adjacent locations close to the main symmetry axis of the plate. The distance between the impact points was approximately 12 mm. The energy of the first impact was equal to 3.9 J, and the energy of the second impact was equal to 6 J.

2.3. Impact damage analysis

Impact damage was analysed using two well-established non-destructive testing (NDT) methods. Ultrasonic C-scan testing and PEXR were used to assess the nature and extent of damage. The former is a full-volume technique capable of providing information about size and depth of internal damage. The plate was ultrasonically C-scanned in pulse-echo mode by a 50-MHz transducer, and the complete ultrasonic waves acquired at each scanning point were processed by selecting the appropriate gate width and position in order to obtain images of the delamination at the desired through thickness depth [20]. The composite plate was scanned from both sides, and the information obtained was recombined to a single three-dimensional image. The extent of damage as reconstructed by C-scan is shown in Figure 3a.

Impact damage was also characterized by means of PEXR. A radio-opaque zinc iodide solution was used to infiltrate the damaged areas before irradiation of the specimen. Radiographic images were obtained on an AGFA NDT D4 film using a HP Faxitron cabinet, with 20-kV voltage, 3-mA current,

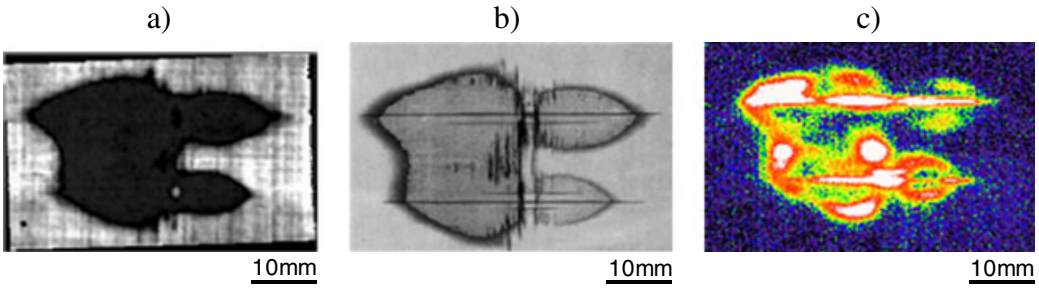

Figure 3. Impact damage revealed by three non-destructive testing methods: (a) ultrasonic C-scan, (b) penetrant-enhanced X-radiography, and (c) vibrothermography.

DOI: 10.1002/stc

and 100-s exposure settings. After processing, digital images of the negative were acquired using an optical scanner. The extent of impact damage as reconstructed using PEXR is shown in Figure 3b. Extensive delaminations at the interface between the 90° and the 0° plies farthest from the impact side (i.e. at the second interface as depicted in Figure 1) is the major damage mode induced by impact. Other fracture phenomena include tensile matrix cracks in 0° plies and shear matrix cracks in the central 90° plies.

3. VIBROTHERMOGRAPHY FOR IMPACT DAMAGE DETECTION

This section describes the vibrothermographic experimental analysis of impact. For the sake of completeness, the first part briefly presents the background of the method. The second part reveals the impact damage in the composite plate.

3.1. Background

Thermography is a family of NDT methods based on temperature measurements to reveal structural damage. All thermographic methods can be divided into two major groups, i.e. passive and active approaches [4]. Passive methods rely on temperature measurements without introducing any external excitation. These methods are rather qualitative and provide global information on potential anomalies. In contrast, active methods require external or internal excitation. The former often uses halogen or flash lamps to heat up a surface of monitored structures. The latter utilizes ultrasound or inductive heating for internal heat generation.

Of special interest in the group of active methods is vibrothermography, also known as thermosonics, sonic infrared or ultrasonic thermography [4–9]. Vibrothermography is a special deployment of active thermography that uses mechanical vibration excitation. The excitation is typically applied using an ultrasonic device that comprises three elements: (1) converter—a bolt clamped Langevin type transducer consisting of piezoceramic stack bolted between two metal pieces (this configuration allows for a high power and narrowband frequency operation); (2) booster—a metal piece (typically aluminium or titanium alloy) that is used to clamp the entire ultrasonic assembly and to amplify vibration amplitude; and (3) sonotrode—an element that comes into contact with inspected structure and further amplifies vibration amplitude. It is important that specific natural frequencies of these elements are perfectly matched for proper operation. Periodic stress waves introduced to a test structure cause frictional sliding at discontinuities (e.g. delaminations, fatigue cracks) and therefore the conversion of mechanical energy into thermal energy generating heat. Thus, the heat source in vibrothermography, unlike in other thermographic techniques, is the discontinuity itself, which makes the identification of defects simpler. Heat generated at discontinuities propagates to the surface where temperature change is measured by a sensitive infrared camera. Typical infrared cameras that are used for this type of tests measure electromagnetic radiation in the medium wavelength infrared spectrum, i.e. from 2.5 to 5 μm. The operation principle of vibrothermography is illustrated in Figure 4.

3.2. Impact damage detection using vibrothermography

Vibrothermography was applied for impact damage detection in the analysed plate. A prototype ultrasonic excitation system (in-house design) and a high performance thermographic camera (Cedip Silver 420M, Wilsonville, Oregon, USA) were used to monitor the composite plate. The ultrasonic generator was operating at 30-W output power and was set to deliver a 28-kHz sinusoidal signal. Amplitude of vibration of the sonotrode at these settings was 3 μm. The excitation was applied outside the field of view of the camera. No coupling has been used between the sonotrode and the test plate that was motivated by the low operating power of the prototype ultrasonic device and therefore no risk of damaging the surface of the plate. The infrared camera was recording temperature evolution at the bottom surface of the plate, i.e. the side opposite to the impacted surface (bottom surface in Figure 1).

The infrared image showing temperature increase, taken 0.5 s after the ultrasonic excitation was introduced to the plate, is presented in Figure 3c. The area of delamination revealed by vibrothermography matches exactly the area revealed by the ultrasonic C-scan and PEXR presented in Figure 3a and Figure 3b, respectively. It has to be noted that no special treatment of the surface of the analysed plate

DOI: 10.1002/stc

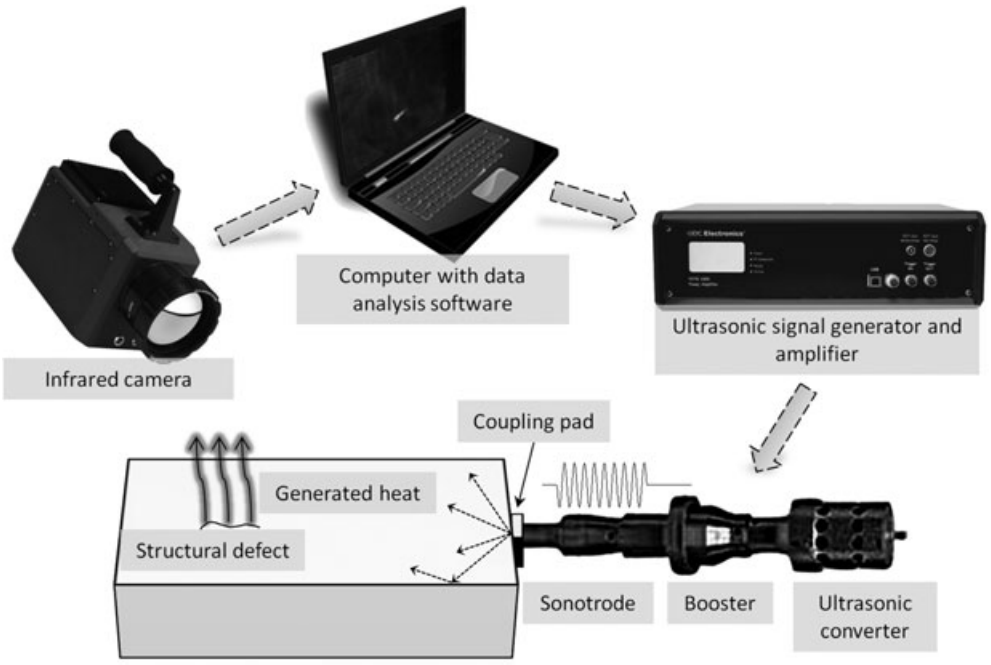

Figure 4. Operational principle of vibrothermography.

was necessary. The calibration of the measurement equipment was also not needed, and the whole measurement took less than 1 min. This makes the vibrothermography a very attractive damage detection technique for applications where inspection time is an issue, as known from many practical applications.

4. FINITE ELEMENT MODEL OF IMPACT DAMAGE

Following experimental investigation in Sections 2 and 3, this section presents modelling of impact damage in the composite plate. The study forms the basis for virtual vibrothermographic test performed in Section 5.

Various modelling approaches can be used to simulate impacts in composites. Finite element (FE) analysis is one of the best approaches for a number of reasons. The most important is that this approach is very well established, and numerous and flexible numerical procedures can be easily expanded and integrated into the existing simulation framework. An explicit time-integration FE modelling has been chosen for this investigation because of the short duration of the impact event and its complex dynamics.

Development of the FE model has been guided by the layout of the experimental setup and properties of the test specimen described in Section 2. FE model has been prepared using the *LS-PrePost* FE (Livermore, California, USA) pre-processor [21]. The model was composed of three main components (Figure 5): (1) rigid post with a rectangular opening; (2) composite plate with $[0_3/90_3]_s$ ply stacking sequence; and (3) rigid indentor with hemispherical tip. The model comprised approximately 1 million

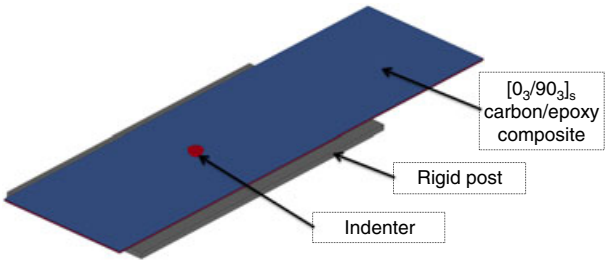

Figure 5. Numerical model used for damage prediction.

DOI: 10.1002/stc

nodes and 832 thousand hexahedral solid elements of which 7.5 thousand were rigid elements. There were four elements across the thickness of the plate—one solid element for every three plies with the same orientation in order to properly reproduce the desired stacking sequence. Average mesh size for the composite plate was 0.5 mm. Simulations have been performed using commercial *LS-DYNA* FE (Livermore, California, USA) software package [22].

Elastic and fracture properties used for the FE model came from previous investigations described in details in [25,26] and are summarized in Table I.

Cohesive elements with zero thickness were applied between 0° and 90° ply interfaces (Figure 1). Although various constitutive equations for the cohesive law have been proposed in the literature to represent the softening and fracture response of an interface a bilinear constitutive law has been employed in this study. The decision was supported by the fact that–according to the literature [27]–numerical results show little sensitivity to the shape of the cohesive law. The traction–separation law in the bilinear model consist of an initial linear elastic stage until a maximum stress is reached followed by a linear softening phase that simulates the progressive decohesion of the interface with increasing damage, as illustrated in Figure 6. Damage occurs when separation reaches a critical value.

In a mixed mode case, i.e. when normal (δ_3) and shear separations (δ_1, δ_2) are non-zero one has to decide how to consider their interaction in the numerical model. In the case investigated, damage is assumed to occur when the quadratic interaction function involving separations reaches a value of 1. A dimensionless effective separation parameter that grasps for the interaction between relative displacements in normal (δ_3—mode I) and tangential (δ_1,δ_2—mode II) directions is defined as:

$$\lambda = \sqrt{\left(\frac{\delta_1}{\delta_{II}^F}\right)^2 + \left(\frac{\delta_2}{\delta_{II}^F}\right)^2 + \left\langle\frac{\delta_3}{\delta_I^F}\right\rangle 2} \tag{1}$$

where δ_{II}^F,δ_{II}^F are critical values representing the maximum separations in normal and tangential directions, respectively, and the Macaulay bracket $\langle\cdot\rangle$ with the usual interpretation is used to distinguish between tension ($\delta_3 \geqslant 0$) and compression ($\delta_3 \geqslant 0$). Graphical representation of the mixed mode behaviour is presented in Figure 7.

Table I. Elastic, fracture and thermal properties of the composite material used.

Mass density	$\rho = 1.6\ \mathrm{g/cm^3}$
Elastic constants	$E_1 = 93.7$ [GPa], $E_2 = 7.45$ [GPa]
	$G_{12} = G_{23} = G_{31} = 3.97$ [GPa]
	$\nu_{12} = 0.261$ [−], $\nu_{21} = 0.0208$ [−]
Thermal expansion coefficients	$\alpha_1 = -0.3 \times 10^{-6}$ [1/K], $\alpha_2 = 28.3 \times 10^{-6}$ [1/K]
Thermal conductivity	$k_1 = 25$ [W/m K], $k_2 = 6$ [W/m K]
Specific heat	$c_p = 700$ [J/kg K]
Fracture toughness	$G_{IC} = 520$ [J/m^2], $G_{IIC} = 970$ [J/m^2]
Peak traction	$k_n = 25$ MPa, $k_s = 65$ MPa

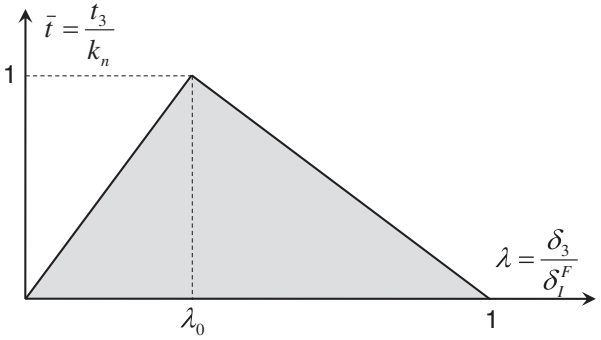

Figure 6. Normalized bilinear traction–separation law for tension.

DOI: 10.1002/stc

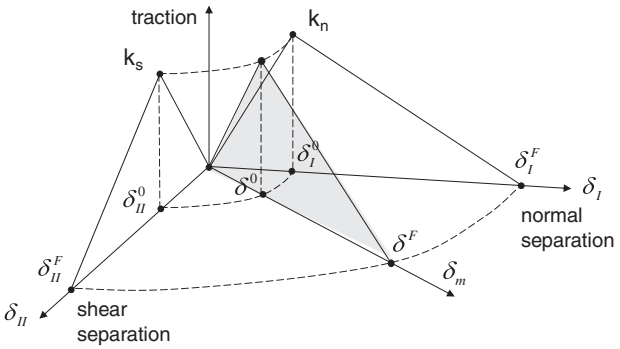

Figure 7. Mixed mode traction–separation behaviour.

$$\left(\frac{|k_{\mathrm{n}}|}{\bar{k}_{\mathrm{n}}}\right)^2 + \left(\frac{|k_{\mathrm{s}}|}{\bar{k}_{\mathrm{s}}}\right)^2 = 1 \tag{2}$$

where k_{n} and k_{s} are the normal and shear stresses on the contact surfaces, respectively, and $\bar{k}_{\mathrm{n}}$ and $\bar{k}_{\mathrm{s}}$ are the normal and shear failure stresses, respectively. The normal and shear failure stresses were set to the same values adopted for cohesive modelling of interface fracture ($\bar{k}_{\mathrm{n}} = 25$ MPa and $\bar{k}_{\mathrm{s}} = 65$ MPa).

Because two subsequent experimental impacts were introduced to the analysed composite plate, numerical simulation had to be performed using two steps. First impact was simulated setting the initial velocity of the indentor so that the energy of impact was equal to 3.9 J. Simulation of the impact event has been performed obtaining partial damage in the plate. To simulate the second impact the composite specimen had to be repositioned with respect to the rigid post. The position of indentor with respect to the post had to remain unchanged as the impact occurred always is in the centre of the opening in the post. Initial velocity of the indentor was increased in order to obtain impact energy of 6 J. Numerical simulations were performed using a single *Intel Xeon 5550* CPU (Santa Clara, California, USA). The total computational time of impact simulation was 80 h (40 h per impact). Figure 8 shows simulated and experimental impact force versus time histories for both impact events. The results show good agreement; the amount of kinetic energy carried by the indentor is properly reproduced in the model.

Numerical simulations were followed by a full analysis of simulated damage. Figure 9 gives the simulated results. The extent of damage can be compared with the experimental results presented in Figure 3, particularly with Figure 3c, where the vibrothermography was used. Extensive delaminations at the interface between the 90° and the 0° plies farthest from the impact side was the major damage mode induced by impact, as expected. The shape and size (Table II) of the simulated and experimental

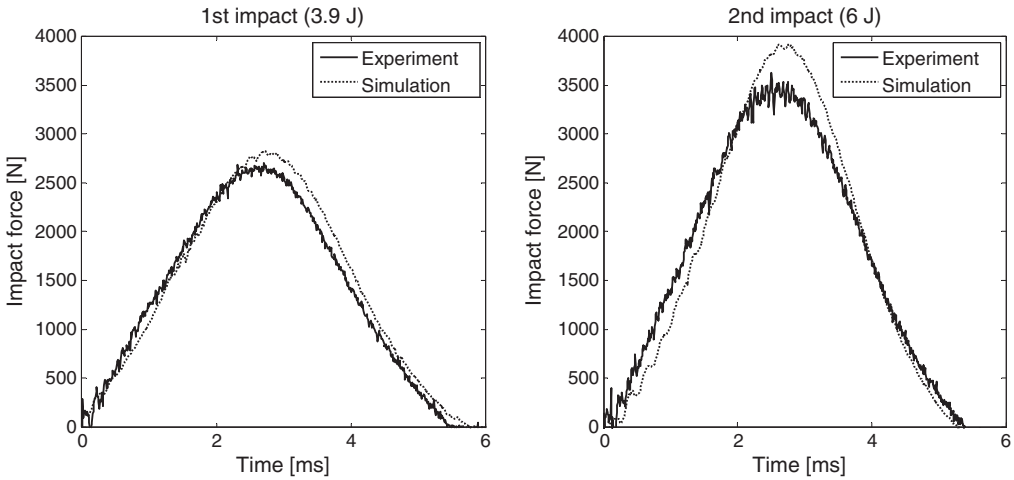

Figure 8. Experimental and simulated impact forces.

DOI: 10.1002/stc

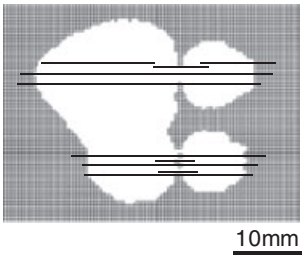

Figure 9. Impact damage revealed by finite element modelling.

Table II. Damage severity estimated from for the vibrothermographic experimental test and numerical simulations.

	Delaminated area [mm^2]	
	Experiment	Simulation
First impact damage	230	213
Second impact damage	330	363
Total area	560	576

delaminations are very similar. Total area of simulated delamination was 576 mm^2. This is very close to the estimated 550 mm^2 area of experimental delamination. It is important to note that the model was able to show that there was no delamination in the areas directly under the indentor. In addition, matrix cracks in 0° plies farthest from the impact side were present in the numerical model. The pattern of cracks is not exactly the same as in the experiment, but this was not expected considering the uncertainties inherent to experimental procedure (e.g. positioning of the plate with respect to the post, non-ideal sphericity of the indenter) and to the laminate itself (e.g. homogeneity of matrix properties, imperfections of the matrix and fibres). In conclusion, modelling and numerical simulations undertaken resulted in good damage prediction if compared with the experimental results.

5. FINITE ELEMENT MODELLING OF VIBROTHERMOGRAPHY IN COMPOSITES

This section describes the main part of the simulated work undertaken. Virtual vibrothermographic test was simulated, following numerical simulations of impact tests.

In order to reproduce the vibrothermographic test numerically, a coupled thermo-mechanical simulation was performed in high frequencies using commercial *LS-DYNA* FE software package [22]. During dynamical loading, the temperature of the material is influenced by three main heat generation mechanisms: thermoelastic effect, thermoplastic effect, and frictional heat generation [23]. Thermoelastic effect is the relationship between the temperature and the applied stress in elastic material. Basic theoretical relation employed for dynamic thermography is

$$\Delta\varepsilon = \frac{(1-2v)\Delta\sigma}{E} + 3\alpha\Delta T \tag{3}$$

where $\Delta\varepsilon$ are changes of main strains, $\Delta\sigma$ are changes of the first stress invariant, v is the Poisson ratio, ΔT are changes of temperature, α is the coefficient of thermal expansion, and E is the Young's modulus.

Thermoplastic effect appears when the yield stress of the material is exceeded. The irreversibility of plastic flow causes an increase in the amount of entropy in the body and the inelastic work is dissipated into heat.

The rate of frictional energy dissipation is given by the product of the frictional stress τ and the slip rate $\dot{\gamma}$:

$$P_{\text{fr}} = \tau \cdot \dot{\gamma} \tag{4}$$

The amount of this energy released as heat on each surface is typically assumed to be the same.

DOI: 10.1002/stc

In this study, thermoplastic effect has not been taken into account because of the non-destructive nature of vibrothermographic measurement [24]. Moreover, considering the short duration of the measurement heat exchange between the specimen and the environment has not been modelled.

Similarly to impact test simulations, the FE model of the measurement setup was prepared using the *LS-PREPOST* FE pre-processor [21]. The FE model consisted of three main components: (1) rigid post; (2) composite plate with $[0_3/90_3]_s$ ply stacking sequence; and (3) rigid cylinder simulating the sonotrode, as shown in Figure 10. The entire model comprised approximately 260 thousand nodes and 202 thousand hexahedral solid elements, of which 900 were rigid elements. There were four elements across the thickness of the plate—one solid element for every three plies—allowing for reproduction of the desired ply stacking sequence.

Simulated impact damage was the starting point for vibrothermographic modelling. Two models for vibrothermographic simulations were prepared. The first model was directly based on the damage state obtained from FE simulation as described in Section 4. The second model was prepared by introducing some modifications—based on the information acquired by PEXR testing—to the results of simulated impact damage. The adjustment included minor reshaping of the delaminated area and repositioning of the cracks to match the experimental data. The motivation behind the preparation of the second model by the enhancement of the computed damage with experimental data was the fact that the simulated damage should resemble the actual damage state in the plate as closely as possible. This gives the possibility of direct comparison of the results of experimental and simulated temperature distributions on the surface of the plate resulting from ultrasonic excitation, as discussed in [10].

Shape and size of the delaminated area at the 0°/90° interface and tensile matrix cracks in the 0° layers have been modelled as surface to surface thermal contact areas as shown in Figure 11. In coupled thermo-mechanical analyses, frictional work can be converted to heat in part or entirely. Additionally, the heat that is generated at the contact interface because of friction can be split equally or unequally between the contacting interfaces. In present model, it has been assumed that the whole frictional work is converted to heat and that the energy dissipated by frictional slip of contact interfaces enters the contacting faces (master and slave) in equal portions. Contact energy at each iteration step was calculated following the *LS-DYNA* procedure as [28]

$$E_{\text{contact}}^{n+1} = E_{\text{contact}}^{n} + \left[\sum_{i=1}^{{}^{n}\text{slave}} \Delta F_i^{\text{slave}} \times \Delta_i^{\text{slave}} + \sum_{i=1}^{{}^{n}\text{master}} \Delta F_i^{\text{master}} \times \Delta s_i^{\text{master}} \right]^{n+\frac{1}{2}} \tag{5}$$

where ^{n}slave is the number of slave nodes, ^{n}master is the number of master nodes, $\Delta F_i^{\text{slave}}$ is the interface force between the ith slave node and respective contact segment, $\Delta F_i^{\text{master}}$ is the interface force between the ith master node and respective contact segment, $\Delta s_i^{\text{master}}$ is the incremental distance the ith slave node has moved during the current time step, and $\Delta F_i^{\text{master}}$ is the incremental distance the ith master node has moved during the current time step. In the absence of friction the slave and master energies should be close in

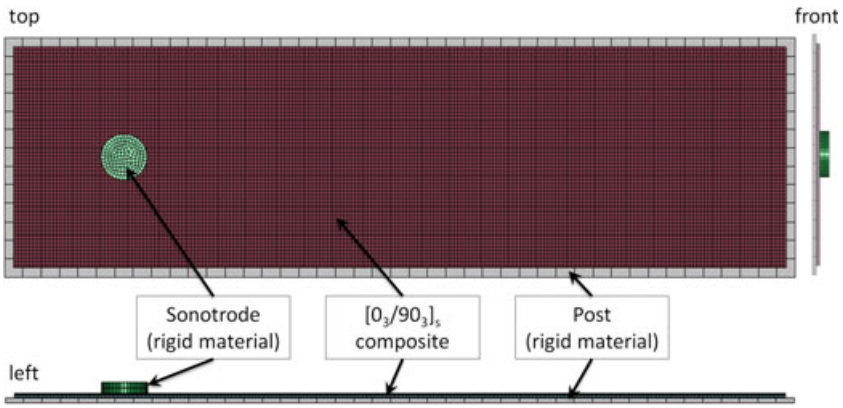

Figure 10. Investigated finite element model of vibrothermographic test.

DOI: 10.1002/stc

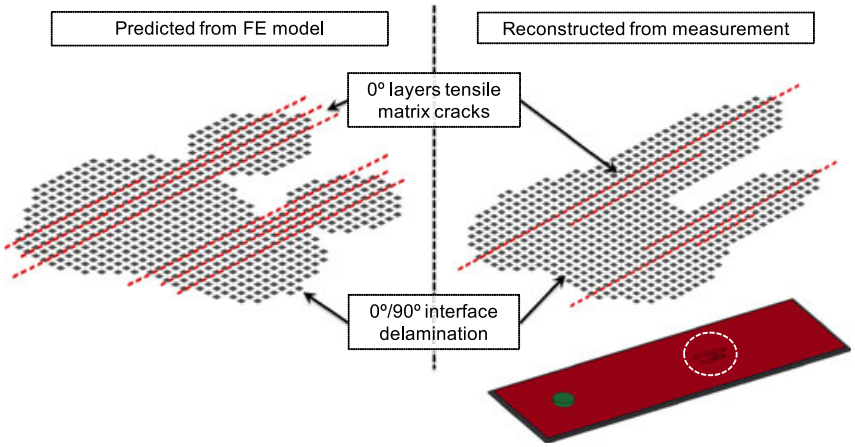

Figure 11. Finite element (FE) damage modelling in the vibrothermographic test.

magnitude but opposite in sign. In the presence of friction, the interface energy can take on a substantial positive value.

Friction in *LS-DYNA* is based on the Coulomb model [28]. In present analysis, the coefficient of static friction μ_s had the value of 0.3, and the coefficient of dynamic friction μ_d had the value of 0.25 for all contact segments in the model. Friction coefficients were assigned based on the limited literature data [29,30]. In order to allow smooth transition between the static and dynamic friction coefficients, an exponential interpolation function was used:

$$\mu = \mu_d + (\mu_s - \mu_d)\mathrm{e}^{-\mathrm{DC}\cdot|v_{\mathrm{rel}}|} \tag{6}$$

where DC is a decay constant and v_{rel} is relative sliding velocity of contact surfaces. Decay constant has been arbitrarily set to 10, but as discussed in [14], the decay constant has virtually no effect on the frictional behaviour in case of close values of μ_s and μ_d as in the considered case. Sliding of contact surfaces occurs when the tangential force is greater than the friction force. Frictional behaviour depends on the characteristics of contact surfaces such as surface roughness or temperature and loading conditions such as normal force and relative velocity.

Transversely isotropic elastic and thermal properties of the composite plate were applied in the numerical model as reported in Table I. There was no information from the manufacturer about thermal properties of the composite. Because it was not possible to perform laboratory tests to obtain the missing thermal parameters of the investigated composite plate, they were estimated based on literature reviews [30–34].

Boundary conditions in the numerical model were specified to represent the experimental setup in the best possible way. Rigid post has been fixed in all degrees of freedom. Contact boundary condition has been was specified between the composite plate and the post. Rigid cylinder modelling the sonotrode was fixed in all degrees of freedom except the translation in z direction (i.e. normal to the composite plate). Translation of the cylinder in z direction was enforced by a sinusoidal displacement boundary condition. Amplitude of vibration was set to 3 μm, and frequency was set to 28 kHz. Coupled field thermo-mechanical analysis has been performed for the duration of 0.2 s. Time step size for the mechanical part was set to 50 ns, and time step size for the thermal part was 100 μs. Thermal time step could be substantially greater than the mechanical time step because of the much slower dynamics of thermal phenomena with respect to ultrasonic wave propagation in the structure. The Crank-Nicolson time integration method [28] was used in solving the heat transfer equation. Numerical simulations were performed using a single *Intel Xeon 5550* CPU. The total computational time was 400 h.

The undamaged area did not exhibit any significant temperature change for all analysed time sequences in experimental measurements and numerical simulations. Figure 12 presents the comparison between experimental and numerical temperature distributions at three different time steps. Images in column *b* in Figure 12 present images from thermographic camera and images in columns *a* and *c* represent simulations. Results in column *a* were obtained from a vibrothermographic simulation on the model with

DOI: 10.1002/stc

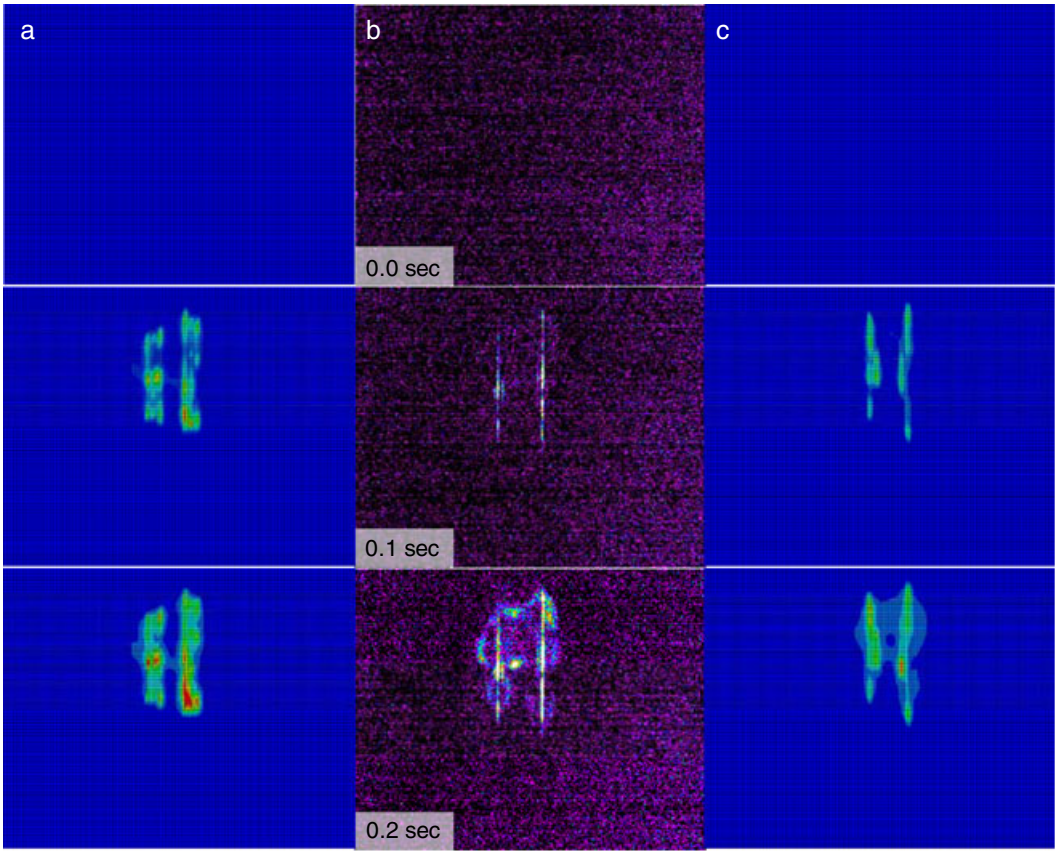

Figure 12. Temperature evolution in the composite plate from the finite element (FE) numerical simulation with predicted damage (column a), vibrothermographic experimental test (column b), and FE numerical simulation with enhanced damage (column c).

damage state predicted from simulations described in Section 4. Results in column *c* were obtained from a vibrothermographic simulation on the model with enhanced damage state as described earlier. Thermographic images in column *b* were obtained by subtracting the first recorded frame from all other frames in the recorded sequence. This allowed the analysis of temperature increase in the plate that was because of the energy dissipated on damage. Uniform temperature distribution on the image at time equal 0 s is the result of the data processing. It can be noticed that measurements contain a noticeable amount of noise coming from the infrared detector, whereas numerical simulations are free of noise. At time equals 0.1 s, it can be seen that only the matrix cracks are visible in thermal image for both experimental data and numerical predictions. For time equals 0.2 s, the whole delaminated area is visible in the measured data (b) and in the model with enhanced damage state (c). In case of numerical results obtained from the model with predicted damage state (a), there was a noticeable amount of heat generated a by surface cracks that made the delaminated area not as clearly visible as in the remaining cases. The time delay between the presence of crack and the presence of delamination in the thermal image is defined by the time necessary for the thermal wave originating from the subsurface delamination to reach the surface. The experimental and simulated results for the damaged area exhibit clear monotonic temperature increase (Figure 13). The simulated results match very well the experimental trend. However, the maximum temperature increase in the damaged area after 0.2 s was equal to 0.1 K in experimental measurements, whereas the equivalent temperature increase in numerical simulations was equal to 0.06 K. The differences between measured response and numerical prediction in the damaged area can be attributed to several factors. First, thermal properties of the composite plate were estimated from literature review and are most likely to be not accurate for the particular composite investigated. Second, friction coefficients were not known precisely for the material used in the current investigations. Third, the damage was modelled approximately using a simple model, i.e. delaminations and cracks were modelled as FE mesh discontinuities (or duplicated

DOI: 10.1002/stc

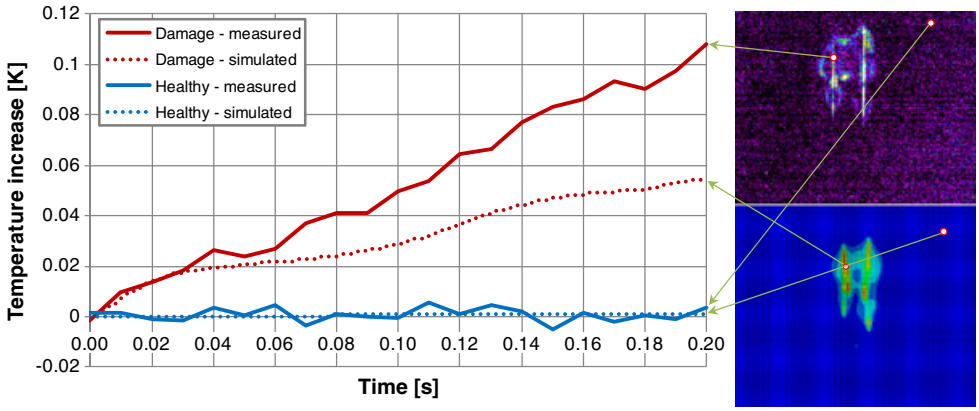

Figure 13. Temperature evolution in selected points on the composite plate obtained from the experimental test (solid lines) and finite element numerical simulations (dotted lines).

nodes) and thermal frictional contact was assumed between the opposite faces. Delamination and crack faces were therefore ideally planar. This assumption does not match reality and certainly influences frictional behaviour. Despite all these discrepancies, the simulation results are very encouraging.

6. CONCLUSIONS

Modelling of vibrothermography for impact damage detection in a composite plate was performed. The study involved two initial experimental impact tests that produce delaminations. The extent of damage was assessed using well-established NDT techniques. Virtual tests were simulated in two steps using FE analysis. First, impact tests were simulated. Second, virtual vibrothermographic test was performed using coupled thermo-mechanical simulation. Simulated results were validated using experimental vibrothermography.

The study shows that it is quite feasible to predict vibrothermographic damage detection results in numerical simulations for impact damage in composite materials. The qualitative agreement between simulated and experimental results was very good. Damage severity/location and temperature trend were assessed correctly using numerical simulations of vibrothermography. However, further work is required to obtain good quantitative temperature agreement. Accurate thermal and frictional characteristics of analysed composites are needed to achieve this task. The authors have learned that obtaining these parameters is in practice a major difficulty. Numerical representation of frictional interfaces could be possibly enhanced using random fields simulating surface roughness as suggested in [20].

Large computational cost of numerical simulations presented in this paper may be of concern in real engineering applications, e.g. for structures where FE models produce large numbers of degrees of freedom. However, this problem could by overcome in the near future by the increasing CPU computational power and by parallelization of FE solvers with use of the General-Purpose computation on Graphics Processing Units (GPGPU) technology.

Vibrothermography has a great potential for Structural Health Monitoring applications. Further research in this area is necessary to better understand the physics behind the method and to make it more reliable allowing for practical applications.

ACKNOWLEDGEMENTS

Research on vibrothermography was financed from the Polish research project MONIT (no. POIG.01.01.02-00-013/08-00).

REFERENCES

1. Inman DJ, Farrar CR, Lopes V Jr, Steffen V Jr (eds.). *Damage Prognosis for Aerospace, Civil and Mechanical Systems*. John Wiley & Sons: Chichester, England, 2005.
2. Staszewski WJ, Boller C, Tomlinson GR (eds.). *Health Monitoring of Aerospace Structures*. John Wiley & Sons: Chichester, England, 2003.

DOI: 10.1002/stc

3. Masters JE (ed.). *Damage Detection in Composite Materials*. ASTM STP 1128 American Society for Testing and Materials: Philadelphia, 1992.
4. Maldague X. *Theory and practice of infrared technology for nondestructive testing*. John Wiley & Sons: New York, USA, 2001.
5. Han X, Favro LD, Ouyang Z, Thomas RL. Recent developments in thermosonic crack detection. *Review of Progress in Quantitative Nondestructive Evaluation* 2002; **21**:552–557.
6. Shepard S. Back to basics: Thermography of composites. *ASNT Materials Evaluation* 2007; **65**(7):690–696.
7. Zweschper T, Dillenz A, Riegert G, Scherling D, Busse G. Ultrasound excited thermography using frequency modulated elastic waves. *Insight-Non-Destructive Testing and Condition Monitoring* 2003; **45**(3):178–182.
8. Shepard SM, Ahmed T, Lhota JR. Experimental considerations in vibrothermography. *Proceedings of SPIE* 2004; **5405**:332–335.
9. Pieczonka LJ, Szwedo M, Uhl T. Detection of structural damages using vibrothermography. IWSHM 7th International Workshop on Structural Health Monitoring, Stanford, CA, 2009.
10. Pieczonka LJ, Staszewski WJ, Aymerich F, Uhl T, Szwedo M. Numerical simulations for impact damage detection in composites using vibrothermography. *IOP Conference Series: Materials Science and Engineering* 2010; **10**(012062):6–7.
11. Plum R, Ummenhofer T. Structural-thermal FE simulation of vibration and heat generation of cracked steel plates due to ultrasound excitation used for vibrothermography. *10th International Conference on Quantitative InfraRed Thermography*, Québec (Canada), 2010.
12. Han X, Islam MS, Newaz G, Favro LD, Thomas RL. Finite-element modelling of acoustic chaos to sonic infrared imaging. *Journal of Applied Physics* 2005; **98**:1–4.
13. Mabrouki F, Thomas M, Genest M, Fahr A. Frictional heating model for efficient use of vibrothermography. *NDT & E International* 2009; **42**:345–52.
14. Han X, Islam S, Newaz G, Favro LD, Thomas RL. Finite element modelling of the heating of cracks during sonic infrared imaging. *Journal of Applied Physics* 2006; **99**.
15. Mabrouki F, Thomas M, Genest M, Fahr A. Numerical modeling of vibrothermography based on plastic deformation. *NDT & E International* 2010; **43**(6):476–483.
16. Saboktakin A, Ibarra-Castanedo C, Bendada A, Maldague X, Bison P, Grinzato E, Marinetti S. Analysis of ultrasonic elastic waves in vibrothermography using FEM. *6th International Workshop-NDT Signal Processing*, London, Ontario (Canada). 2009.
17. Bolu G, Gachagan A, Pierce G, Harvey G. Reliable thermosonic inspection of aero engine turbine blades. *Insight - Non-Destructive Testing and Condition Monitoring* 2010; **52**(9):488–493.
18. Mian A, Han X, Islam S, Newaz G. Fatigue damage detection in graphite/epoxy composites using sonic infrared imaging technique. *Composites Science and Technology* 2004; **64**(5):657–666.
19. Mian A, Newaz G, Han X, Mahmood T, Saha C. Response of sub-surface fatigue damage under sonic load—a computational study. *Composites Science and Technology* 2004; **64**(9):1115–1122.
20. Aymerich F, Meili S. Ultrasonic evaluation of matrix damage in impacted composite laminates. *Composites Part B: Engineering* 2000; **31**(1):1–6.
21. Livermore Software Technology Company. LS-PrePost—Online documentation. Available from: http://www.lstc.com/lspp/ [December 2010].
22. Livermore Software Technology Company. LS-Dyna Keyword User's Manual. 2009.
23. Harwood N, Cummings WM. *Thermoelastic Stress Analysis*. IOP Publishing: Bristol, 1991.
24. Tsoi KA, Rajic N. Effect of sonic thermographic inspection on fatigue crack growth in an Al alloy. *DSTO–TN–0584*, 2004.
25. Aymerich F, Dore F, Priolo P. Prediction of impact-induced delamination in cross-ply composite laminates using cohesive interface elements. *Composites Science and Technology* 2008; **68**:2383–2390.
26. Aymerich F, Dore F, Priolo P. Simulation of multiple delaminations in impacted cross-ply laminates using a finite element model based on cohesive interface elements. *Composites Science and Technology* 2009; **69**:1699–1709.
27. Alfano G. On the influence of the shape of the interface law on the application of cohesive-zone models. *Composites Science and Technology* 2006; **66**:723–730.
28. Livermore Software Technology Company. LS-Dyna Theory Manual. 2006.
29. Chand N, Fahim M. *An introduction to tribology of FRP materials*. Allied Publishers: New Delhi, India, 2000.
30. Gay D, Hoa SV, Tsai SW. *Composite Materials Design and Applications*. CRC Press: Boca Raton, USA, 2003.
31. Melo JD, Radford DW. Determination of the elastic constants of a transversely isotropic lamina using laminate coefficients of thermal expansion. *Journal of Composite Materials* 2002; **36**:1321–1329.
32. The Japan Carbon Fiber Manufacturers' Association. Available from: http://www.carbonfiber.gr.jp/english/ [December 2010].
33. National Physical Laboratory. Available from: http://www.kayelaby.npl.co.uk/ [March 2011].
34. Shim HB, Seo MK, Park SJ. Thermal conductivity and mechanical properties of various cross-section types carbon fiber-reinforced composites. *Journal of Materials Science* 2002; **37**(9):1881–1885.

DOI: 10.1002/stc